Moho topography beneath the Corinth Rift area (Greece) from inversion of gravity data

C Tiberi, M Diament, H Lyon-Caen, T King

Geophys. J. Int. (2001) **145,** 797–808

Moho topography beneath the Corinth Rift area (Greece) from inversion of gravity data

C. Tiberi,[1]* M. Diament,[2] H. Lyon-Caen[3] and T. King[4]

[1] *Département de Sismologie, IPGP,* 4 *Place Jussieu,* 75252 *Paris Cedex* 05*, France*
[2] *Laboratoire de Gravimétrie et Géodynamique, IPGP,* 4 *Place Jussieu,* 75252 *Paris Cedex* 05*, France*
[3] *Laboratoire de Géologie, ENS,* 24 *Rue Lhomond,* 75231 *Paris Cedex* 05*, France*
[4] *Esso UK Ltd, Department of Exploration, Mailpoint* 25*, Esso House, Ermyn Way, Leatherhead, Surrey,* KT22 8UY, *UK*

Accepted 2001 February 9. Received 2000 February 5; in original form 2000 October 18

SUMMARY

Our aim is to understand better the rifting process by imaging the Moho depth variation beneath Corinth and Evvia. We present here the results of a gravity inversion analysis in the region of the Corinth and Evvia rift system, and compare them to those obtained independently from teleseismic tomography and receiver function analyses. The results of these different studies appear to be consistent and show (1) a 10 km crustal thickening in the western part of the area beneath the Hellenides mountains, (2) NW–SE-trending periodic crustal thinning, and (3) a maximum crustal thinning north of the Gulf of Corinth. This 4 km thinning is unlikely to be the result of the rifting alone, which seems to have been reactivated since only 1 Ma. We propose here a geodynamical scenario in two major steps to explain the evolution of Corinth area. Aegean Miocene extension involving boudinage resulted in periodic crustal thinning, consistent with observations. These lithospheric instabilities could have favoured rupture initiation in particular areas, especially near the city of Corinth. Then, the reactivation of the Corinth Rift extension, 1 Myr ago, led to westward rift propagation. The offset observed between the maximum crustal thinning and the Gulf of Corinth could be accommodated by a low-angle normal fault at about 10–15 km depth. The Corinth Rift is thus asymmetrical and was initiated in places of crustal weakness due to Miocene lithospheric instabilities.

Key words: boudinage, continental rifts, gravity inversion, Greece, Moho discontinuity.

1 INTRODUCTION

Lithospheric processes controlling the initiation and evolution of continental rifting are still barely constrained and remain debated (see e.g. Ruppel 1995, for an overview). The understanding of the geodynamical evolution of rifting areas requires one to discriminate between different modes of rifting: pure shear, simple shear or a combination of the two mechanisms. In pure shear mode, uniform and symmetrical thinning of the entire lithosphere occurs by continuous deformation rather than by faulting (McKenzie 1978b), whereas the simple shear mechanism is characterized by brittle faulting and localized strain along fault zones (Wernicke 1985). The latter is often associated with lithospheric low-angle normal or listric faults, and results in an offset between crustal thinning and mantle rising. The combination of pure shear and simple shear usually incorporates low-angle faulting in the brittle crust and ductile stretching in the lower crust (Lister & Davis 1989). These rifting modes involve totally different deep-seated mechanisms, and their relations to surficial structures are not obvious (e.g. Allemand & Brun 1991; Brun & Beslier 1996).

Therefore, imaging the lithospheric structures helps to distinguish between rifting modes. For example, the Moho topographic variation helps to localize the maximum crustal thinning. Inversion of gravity data is an efficient tool to obtain this information, and it offers an opportunity to shed light on rifting processes when applied to present-day active rift zones (e.g. Petit *et al.* 1997; Mahatsente *et al.* 1999).

The Aegean region, where rapid continental extension is currently observed (e.g. Le Pichon *et al.* 1995; Clarke *et al.* 1998) is a key place to study rifting processes. In this paper, we focus on one of the most seismically active areas of the Aegean: the

* Now at: Geology Department, Royal Holloway, University of London, Queen's Building, Egham, Surrey, TW20 0EX, UK. E-mail: c.tiberi@gl.rhul.ac.uk

Corinth and Evvia rift system, where deformation is localized (e.g. Clarke *et al.* 1998; Briole *et al.* 2000). Many of the active structures are above sea level, making this an excellent location to study continental extension.

We take advantage of the good coverage of the area with gravity observations to map the Moho variations in the Corinth region. This topography is obtained using an iterative scheme based on the method of Oldenburg (1974). We investigate the influence of additional sources of density anomalies, such as the subducted oceanic lithosphere of the African plate beneath the southern Aegean. Our results are then compared to those of two independent studies carried out in the same area. The first comes from teleseismic tomography, which gives us velocity variations down to 200 km. The second comes from a receiver function analysis along a 180 km profile. Combining the results from these three complementary techniques enables us to gain new insight into the Corinth Rift evolution and the geodynamical evolution of the Aegean region.

2 GENERAL SETTING

The Aegean area is believed to have been extending since Miocene times (e.g. Le Pichon & Angelier 1979; Mercier 1981). Extension today is very rapid (3 cm yr^{-1} relative to Eurasia; McClusky *et al.* 2000), there is much seismic activity and many rifting-related structures are exposed at the surface. Extension was initiated 15 or 20 Myr ago, probably by a gravitational collapse of the Hellenides mountains (Le Pichon *et al.* 1995), which immersed the central part of the Aegean region and created the Aegean Sea. At present, dynamic processes at boundaries could maintain the extension, but how they relate to it is still a matter of debate (e.g. Armijo *et al.* 1996; Lundgren *et al.* 1998). The Aegean is bounded to the south and west by the Hellenic arc (Fig. 1). The African plate is moving northwards at about 0.5 cm yr^{-1} relative to Eurasia (McClusky *et al.* 2000). The Anatolian block to the east of the Aegean is rotating counter-clockwise about a pole near the Nile Delta as it is extruded westwards (McKenzie 1978a; Barka 1996). Part of this motion is accommodated along the right-lateral strike-slip North Anatolian fault moving at about 2 cm yr^{-1} (McClusky *et al.* 2000).

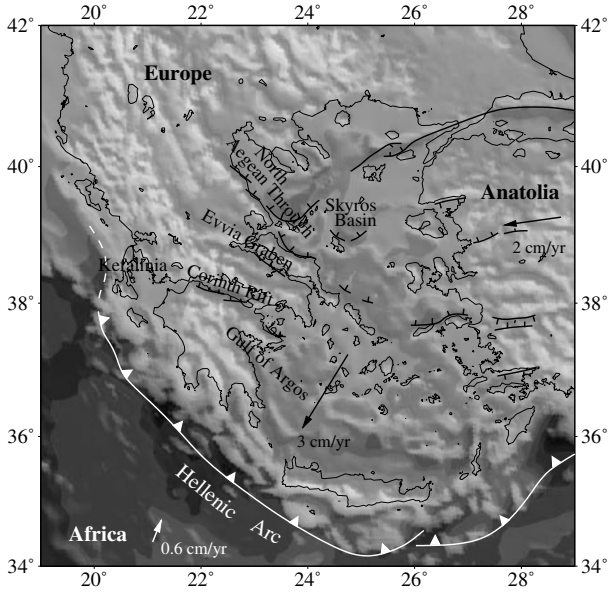

Figure 1. Simplified geodynamical sketch for the Aegean region. The arrows indicate the direction of movement relative to Eurasia (velocities after McClusky *et al.* 2000). Topography is from the ETOPO5 model and shows the main relief in Greece.

The surface expression of the Aegean extension is presently localized on a series of rifts that are less than 50 km wide (Armijo *et al.* 1996; McClusky *et al.* 2000) and which seem to have a periodic spacing of about 70 km (Armijo *et al.* 1996) (Fig. 1). The Corinth Rift, which separates the Peloponnesus from Central Greece, is one of the most active of these structures (e.g. Jackson *et al.* 1982; Bernard *et al.* 1997). This ESE–WNW 130 km long asymmetrical graben crosses the NNW–SSE-trending fabric of the Hellenides, and is bounded by well-exposed Quaternary faults. These faults are likely to be responsible for the large earthquakes that occur in the area (e.g. Ambraseys & Jackson 1990; Papazachos & Kiratzi 1996). The focal mechanisms and surface rupture in the Corinth Rift mainly correspond to normal faulting associated with N–S extension, consistent with recent GPS results (Briole *et al.* 2000). More generally, geodesy reveals an average extension rate over the last 100 years of approximately 1 cm yr^{-1} in a N10E direction (Billiris *et al.* 1991). The asymmetry of this graben is particularly obvious from the surface expression of the faulting system. The most active faults are located on the southern uplifted edge, whereas minor antithetic faults are concentrated on the northern subsided edge. The southern faulting system is organized *en echelon* with segments of 15–25 km long, and shows a northward dip of about 50° near the surface (Armijo *et al.* 1996). The system has migrated northwards during the evolution of the rift (Ori 1989; Sorel 2000), and a connection with a low-angle detachment fault plane at depth is suspected in the western part of the rift (Rietbrock *et al.* 1996; Bernard *et al.* 1997; Sorel 2000). On the basis of a larger amount of finite extension in the eastern part of the Gulf and larger extensional strain in the western part of the Gulf (0.15 ppm yr^{-1} to the east versus 1.12 ppm yr^{-1} to the west; Clarke *et al.* 1998), it seems likely that the extension has propagated westwards during the evolution of the rift. The Corinth Rift seems to have formed mainly during the Quaternary. Armijo *et al.* (1996) proposed that the extensional rate abruptly increased 1 Myr ago due to the influence of the westward propagation of the Anatolian fault. The Evvia Rift north of Corinth is another asymmetrical graben (e.g. Roberts & Jackson 1991). Although it is less active, it still accommodates part of the deformation in the region (e.g. Clarke *et al.* 1998).

Although several geological and geophysical studies have been carried out on the Corinth and Evvia rifts (e.g. Bonneau 1982; Hubert *et al.* 1996; Rigo *et al.* 1996; Bernard *et al.* 1997; Sorel 2000), how the surface expression of these continental rift areas is related to deep lithospheric processes remains largely unknown. New insights were recently obtained from a teleseismic tomography study across the Corinth and Evvia region (Tiberi *et al.* 2000). In this study, the African slab was imaged between 70 and 200 km depth, and there was evidence for crustal thinning north of the Corinth Gulf. This Moho variation was also revealed by a recent receiver function analysis in the same area (Schubnel 1999). However, the poor vertical resolution of the tomography in the crust and the limited size of the study did not allow for an accurate determination of the amount of crustal thinning. New information about the lithosphere, particularly variations in Moho topography, is therefore essential to improve our understanding of the region.

3 MOHO VARIATIONS BENEATH THE CORINTH RIFT AREA FROM GRAVITY

3.1 Data analysis

The gravity data across the Corinth and Evvia region were collected and collated by TK. Numerous sources and surveys were used, including various onshore data sets made available by the Greek Institute of Geology and Mineral Exploration (IGME) and the University of Athens, marine gravity data across the Gulf of Corinth (made available by M. Brooks), and data from two field seasons in Greece. All sources were calibrated and tied to the IGSN71 standard (King 1998; King *et al.* 2000). All data were reprocessed to a common standard from measurements of position, observed gravity and elevation. The estimated error in the simple Bouguer anomaly is less than 1 mGal for all sources. The largest source of error came from the terrain correction, and the error in the complete Bouguer anomaly is ± 4 mGal. The resulting data set is evenly distributed over the studied area (Fig. 2). Some regions are more densely covered than others (e.g. the southwestern part of Peloponnesus and the northwestern part of Evvia island), whereas no data are available offshore in the Gulf of Evvia. The Gulf of Corinth and the surrounding regions are well sampled, providing good model constraints in this area. A map of the complete Bouguer anomaly is shown in Fig. 3. The most striking feature is the strong E–W gradient of approximately 1 mGal km^{-1}. Smaller wavelengths are superimposed, especially in the Beotian area and around the Corinth and Evvia rifts.

We are interested in the overriding Aegean lithosphere, but density contrasts due to the subducted African lithosphere are likely to create a significant gravity signal (Tsokas & Hansen 1997). The gravity effect of the African slab was computed by Tsokas & Hansen (1997). They used a somewhat arbitrary slab geometry defined by Gregersen & Jæger (1984) to model the resulting gravity field. We choose here to compute the gravity anomaly due to the subducted slab using the available seismological data and a linear relation between velocity and density

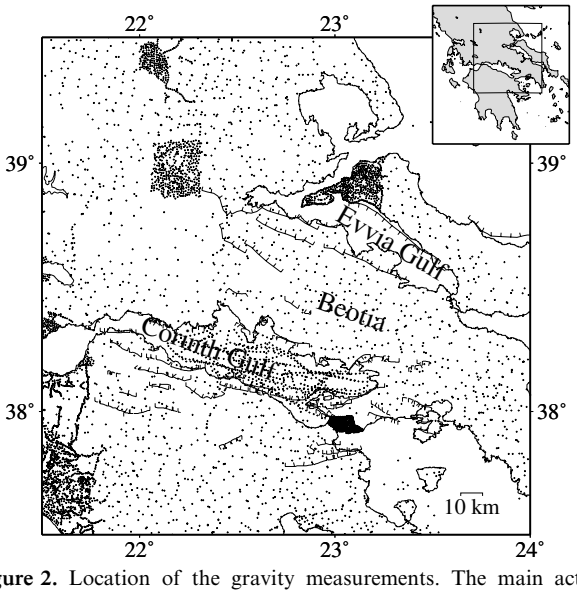

Figure 2. Location of the gravity measurements. The main active faults of the Corinth area are shown (Roberts & Jackson 1991; Armijo *et al.* 1996).

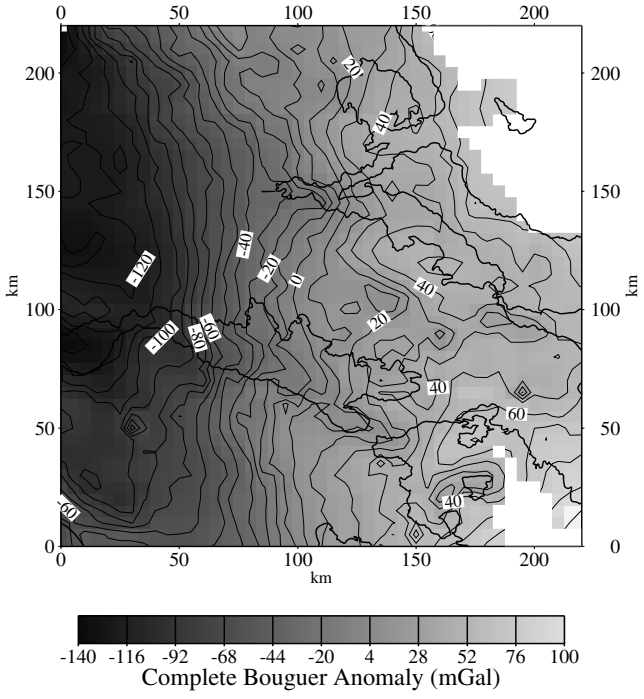

Figure 3. Complete Bouguer anomaly map in mGal (isolines every 10 mGal). Coordinates are expressed in the UTM system (km).

(e.g. Birch 1961). For this purpose, we use the Aegean part of the large-scale tomographic model of Bijwaard *et al.* (1998), which is derived from 7.5×10^6 *P* and *pP* arrival times. The cell size is 0.6° in latitude and longitude and the boundaries are distant enough to be free from edge effects (750×750 km^2 area). The slab is defined here by cells with a positive velocity perturbation between 70 and 350 km depth. The magnitude of the velocity perturbation is less than 5 per cent of the initial velocity model used by Bijwaard *et al.* (1998).

To compute the gravity effect of the African subducted lithosphere from this velocity model, we first tried the linear relation between density (ρ) and *P*-wave velocity (V_p) of Henkel *et al.* (1990) for mantle rocks,

$$V_p = 2.61\rho - 1.00\,. \tag{1}$$

However, using this relation, we obtain a value of $\rho =$ 120 kg m^{-3}, twice the density usually taken for a slab (e.g. Truffert *et al.* 1993). Indeed, eq. (1) does not include the effects of pressure or temperature, and according to Christensen & Mooney (1995), the effect of pressure alone is to double the linear coefficient of eq. (1). As a result, we use the following relation between velocity variation ΔV_p and density variation $\Delta\rho$:

$$\Delta V_p = 5\Delta\rho\,. \tag{2}$$

For a velocity perturbation of 4 per cent, eq. (2) yields a density contrast of about 60 kg m^{-3}. Fig. 4 presents the gravity anomaly computed from the tomographic model and eq. (2). The slab effect results in a positive anomaly, centred northeast of the Hellenic trench. For the Corinth and Evvia region (Fig. 4b), the gradient is about 10 mGal per 50 km. Although the shape of the anomaly is similar to that computed by Tsokas & Hansen (1997), we obtain a gradient twice as large. This is mostly due to the different geometry we used. The slab from Bijwaard *et al.* (1998) dips more steeply than that of Gregersen

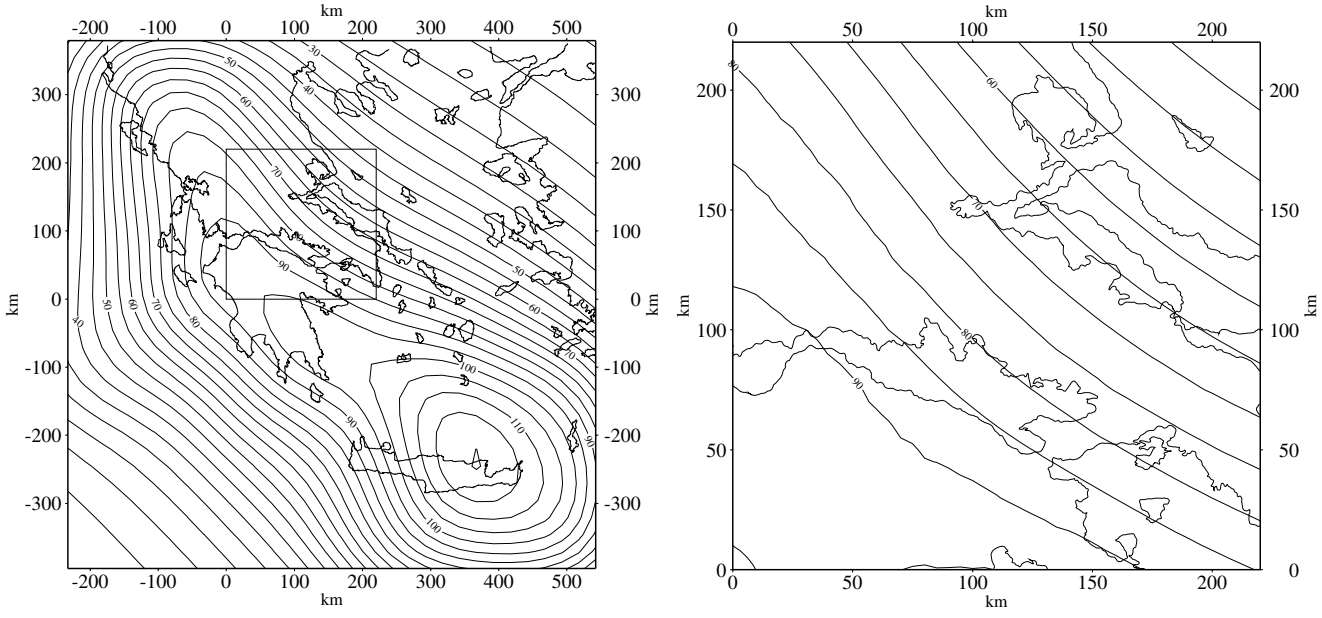

Figure 4. Computed gravity anomaly due to the African slab in mGal. Coordinates are expressed in the UTM system. Gravity anomaly (a) for the whole Aegean region and (b) for the Corinth an Evvia area. The geometry of the slab is taken from the tomographic model of Bijwaard *et al.* (1998) and we use a linear relation between velocity and density contrast (see eq. 2). Isolines every 5 mGal.

& Jæger (1984). Additionally, eq. (2) results in a varying density inside the slab, whereas Tsokas & Hansen (1997) used a constant 60 kg m^{-3} contrast.

By removing the gravity effect of the African slab from the complete Bouguer anomaly, we obtain the residual anomaly shown in Fig. 5(a). For our purpose, only the variations of the residual anomaly are meaningful. We have thus offset the residual anomaly to make it positive everywhere. The strong west to east gradient is still present (Fig. 5a). As the gravity field of the slab is primarily a linear gradient, precise knowledge

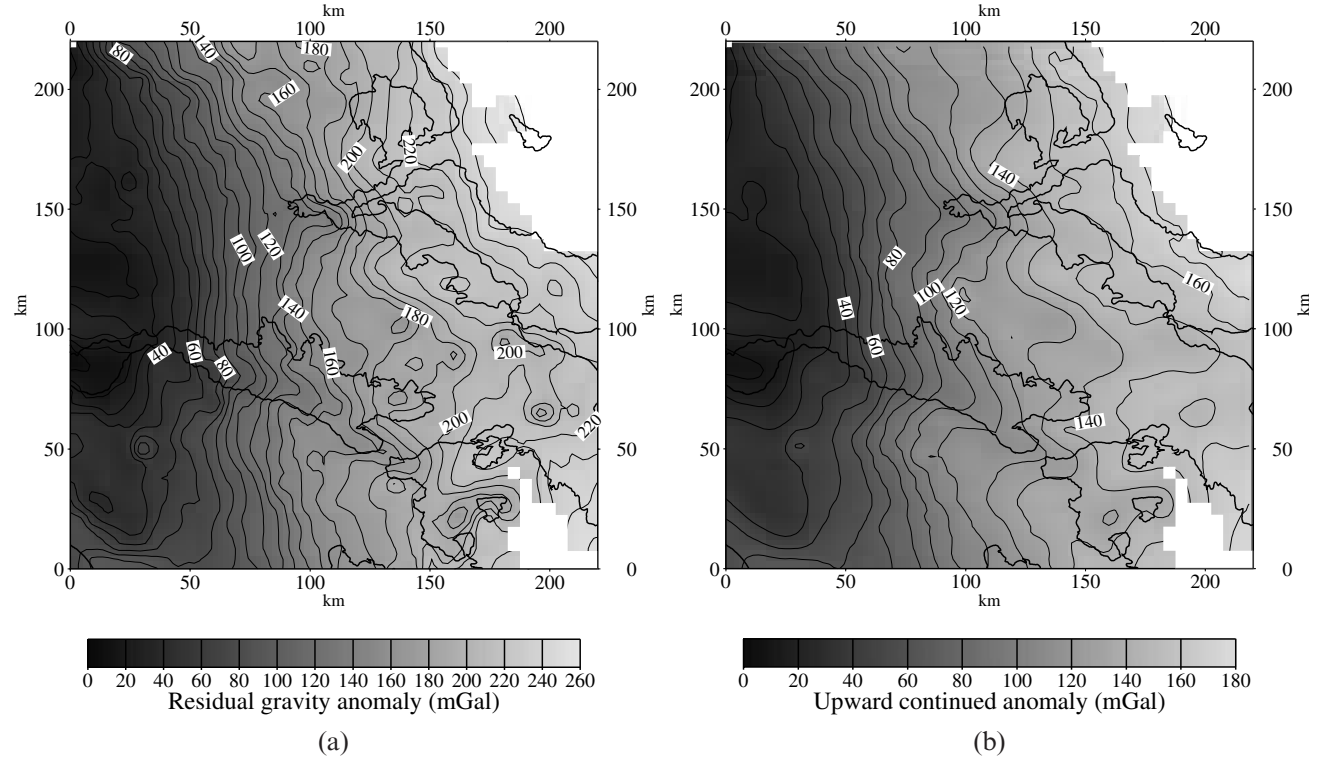

Figure 5. (a) Residual anomaly (mGal) obtained after removing the slab effect from the complete Bouguer anomaly. (b) Upward continuation of the residual anomaly to a constant altitude of 4 km asl. Isolines every 10 mGal; coordinates are expressed in the UTM system.

of its geometry is unnecessary. Moreover, tests show that its removal from the complete Bouguer anomaly has negligible effect on the inversion results.

To reduce finally the shortest wavelengths coming from shallow and small geological structures, we continue the residual anomaly upwards to a constant altitude of 4 km asl (Ciminale & Loddo 1989). The resulting residual anomaly is shown in Fig. 5(b). The strong gradient and the long wavelengths are still preserved, and significant variations north and south of the Corinth Rift are clearly observed. We now assume that the residual anomaly in Fig. 5(b) is due to the Moho topography.

3.2 Method

To obtain the Moho topography, we apply the Oldenburg (1974) method to the residual anomaly (Fig. 5b). This approach was successfully applied in a recent study of the Aden region by Hébert *et al.* (2000). The assumption is that the inverted gravity anomaly reflects only the Moho topography. A low-pass filter is used to stabilize the inversion and to get rid of the remaining short wavelengths coming from the shallow crustal structures. In our case, wavelengths shorter than 55 km are suppressed, and those between 55 and 75 km are scaled by a cosine taper. For more details, see the original article of Oldenburg (1974).

The iterative process is applied in the spectral domain and uses the direct formula of Parker (1972), where the gravity anomaly, $\Delta g(x, y)$, is linked to the topography of the interface, $h(x, y)$, around an average depth, z_0, by

$$\mathcal{F}(h(x, y)) = \frac{\mathcal{F}(\Delta g(x, y))\, e^{|k|z_0}}{2\pi G \Delta\rho} - \sum_{n=2}^{\infty} \frac{|k|^{n-1}}{n!}\, \mathcal{F}(h^n(x, y)), \quad (3)$$

where $\mathcal{F}$ represents the Fourier transform, G is the gravitational constant, k is the wavenumber and $\Delta\rho$ is the density contrast at the interface $h(x, y)$. Moho depth $z(x, y)$ is then defined by

$$z(x, y) = z_0 + h(x, y). \quad (4)$$

The maximum value for n used here is 4. Our tests have shown that taking into account higher-order terms is meaningless. We also carried out several synthetic tests in two and three dimensions to detect possible artefacts and to investigate the influence of the various parameters (see Appendix A).

According to seismic studies in the Aegean and continental Greece (Makris 1978; Papazachos & Nolet 1997), we choose a reference Moho depth z_0 of 30 km. We use 450 kg m^{-3} for the crust–mantle density contrast. Tests were made with different values for z_0 and $\Delta\rho$ ($z_0 = 26$ and 36 km and $\Delta\rho = 350$ kg m^{-3}), and the results appear to be robust (see Appendix B).

3.3 Results and comparison with seismological analysis

The inversion of the residual anomaly (Fig. 5b) converges after four iterations with an rms of 2.61 mGal. The resulting Moho topographic variations (about $z_0 = 30$ km) are presented Fig. 6(a) and the residual gravity anomaly is shown Fig. 6(b). Although locally in some areas residuals of up to 15 mGal are present, most of the residuals are within ± 4 mGal, which is the magnitude of the initial error in the data. Considering a 15 km wide and 5 km high Moho topographic variation at 30 km depth, a residual of about 6 mGal corresponds to a 2 km error on the maximum Moho depth location.

The resulting Moho topography shows that NW–SE-trending features (about 15 km wide) are superimposed on a general crustal thickening towards the west. In the western part of the region, the Moho is about 13 km deeper than the reference value (30 km). Even if there are some short-wavelength artefacts in this area (see Appendix A), the general crustal thickening is very clear. North and south of the Gulf of Corinth and in the Evvia region, we observe two well-defined areas with a shallow Moho at about 25 km depth. The Moho depth beneath the northern edge of the Corinth Gulf may be even shallower than 25 km, as the corresponding residual is high in this region (about +15 mGal, Fig. 6b). These NW–SE-trending zones of shallow Moho are spaced at about 60 km. This pattern is preserved when varying parameters of the inversion (filter, $\Delta\rho$, z_0) and thus cannot be an inversion artefact (see Appendix B).

It is now possible to compare these results with those obtained from the 1996 seismological study (Tiberi *et al.* 2000). More than 2300 teleseismic first arrivals were inverted to obtain a tomographic model of the lithosphere down to 200 km depth (Tiberi 1999). The ACH method of Aki *et al.* (1977) revised by Evans & Achauer (1993) was used. Fig. 7 shows the tomogram obtained in the layer between 25 and 40 km. Fast velocities are represented in blue colours and low ones in red. As tomography gives here the mean velocity for the layer between 25 and 40 km, a fast velocity indicates the location of crustal thinning, whereas a low velocity is characteristic of thicker crust (Tiberi *et al.* 2000). We do not attempt here to make quantitative correlation between gravity and seismological results, as tomography fails in giving the absolute Moho depth value (Tiberi *et al.* 2000). Thus, we discuss here a visual correlation between Figs 6 and 7. The comparison between the gravity results and the tomographic model shows that regions of deeper (shallower) Moho modelled from gravity inversion coincide with zones of low (fast) velocity (Fig. 7b). In particular, the main low-velocity contrast of about −5 to −7 per cent perturbation in Fig. 7(a) at the southwestern part of the network [present in both the upper (10–25 km depth) and the lower (40–65 km) tomograms] corresponds to a deep Moho according to gravity inversion (Fig. 6). Similarly, a good correlation is observed between the NW–SE-trending 15 km wide velocity perturbation located north of the Corinth Gulf and the shallow Moho area obtained from gravity inversion. The velocity contrast in tomography roughly corresponds a 5 km shallower Moho. This is consistent with the 4 km obtained from gravity (Fig. 6).

The correlation is less obvious in the Evvia area, and may result from poor resolution of gravity and tomography inversions. South of the Gulf of Corinth, the gravity inversion yields a Moho about +4 km shallower that seems to be correlated with a fast but weak velocity perturbation on the tomogram (Fig. 7). The weakness of this perturbation may be due to the adjacent very low velocities (Tiberi *et al.* 2000).

A receiver function analysis was also performed using the data of this 1996 experiment (Schubnel 1999). 22 teleseismic events recorded by the three-component broad-band seismometers (CMG40–20 s) of the westernmost profile were used (12 seismological stations, Fig. 8). Epicentral distances range between 30° and 95° and azimuths range between 20° and 250°. The main results of this analysis are reported in Fig. 8 on a tomogram cross-section summarizing the Moho depths beneath the western profile from both receiver function analysis and gravity inversion.

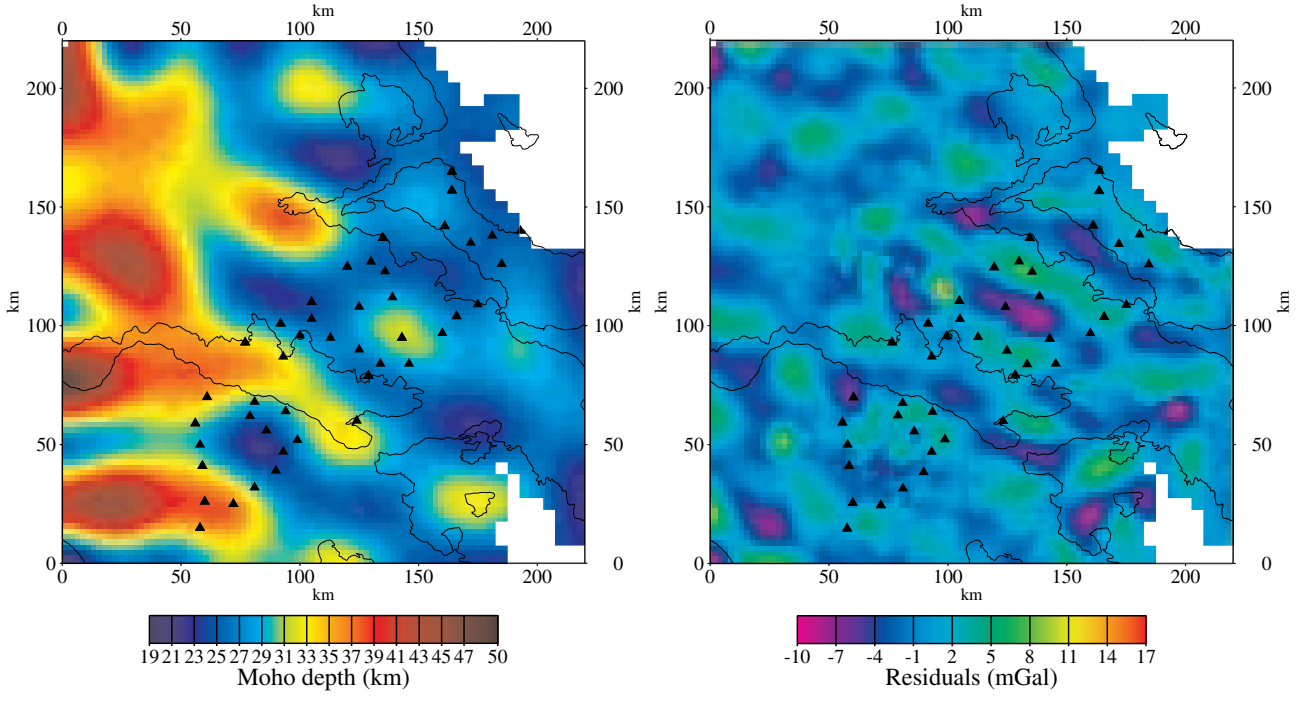

Figure 6. (a) Moho depth (in km) obtained from the inversion of the residual gravity anomaly of Fig. 5(b). The red colours indicate deeper Moho and blue colours shallower Moho. (b) differences in mGal between the observed anomaly of Fig. 5(b) and the computed gravity anomaly produced by the topography of Fig. 6. The black triangles represent the seismological stations of the 1996 seismological experiment in this area. Residuals are between ± 4 mGal, similar to the accuracy of the data. The coordinates are expressed in the UTM system.

Fig. 8 shows that Moho variations according to the receiver function analysis are consistent with those obtained from our gravity inversion. Crustal thinning and thickening are systematically found at the same location. The depth difference between the two methods is everywhere less than 3 km. The crustal thickness is largest in the southern part of the profile, where the Moho depth reaches about 37 km beneath station ELAT (36.5 km from the receiver function analysis and 37 km

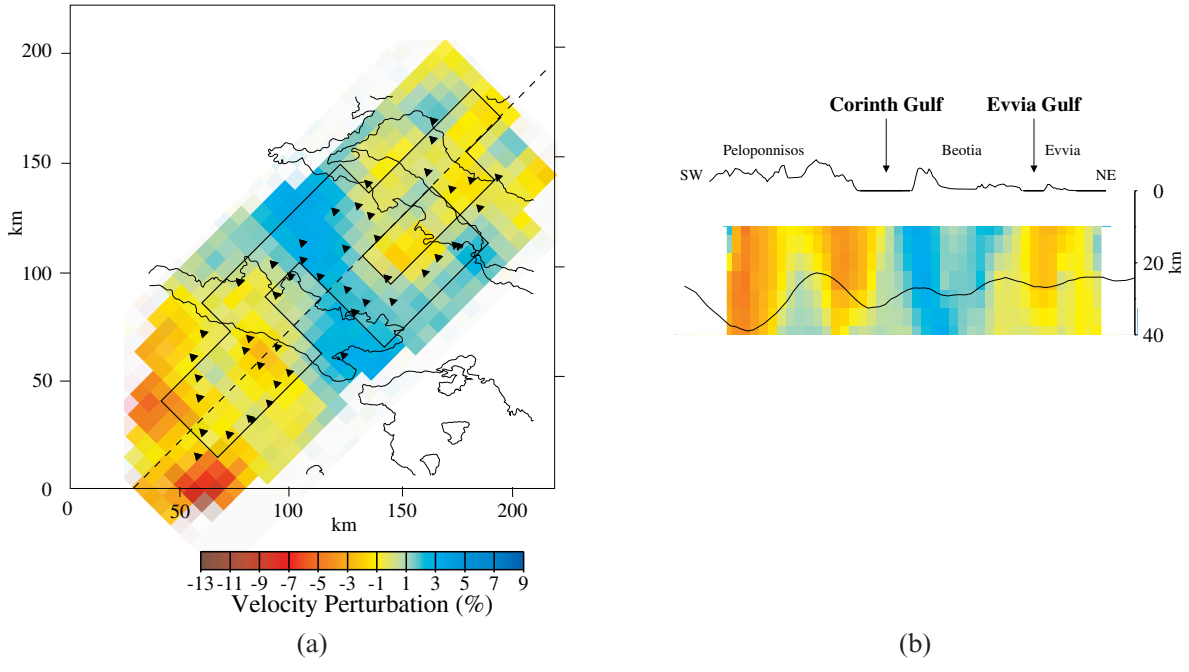

Figure 7. (a) Tomogram at about 30 km depth obtained from a teleseismic inversion of *P* and *PKP* traveltimes (Tiberi *et al.* 2000). The station location is indicated by the black triangles and the thick black line represents the 0.5 resolution limit for the inversion. (b) Vertical cross-section through the network (long dashed line in a) from 0–40 km depth showing tomographic results and Moho topography from the gravity inversion (black thick line).

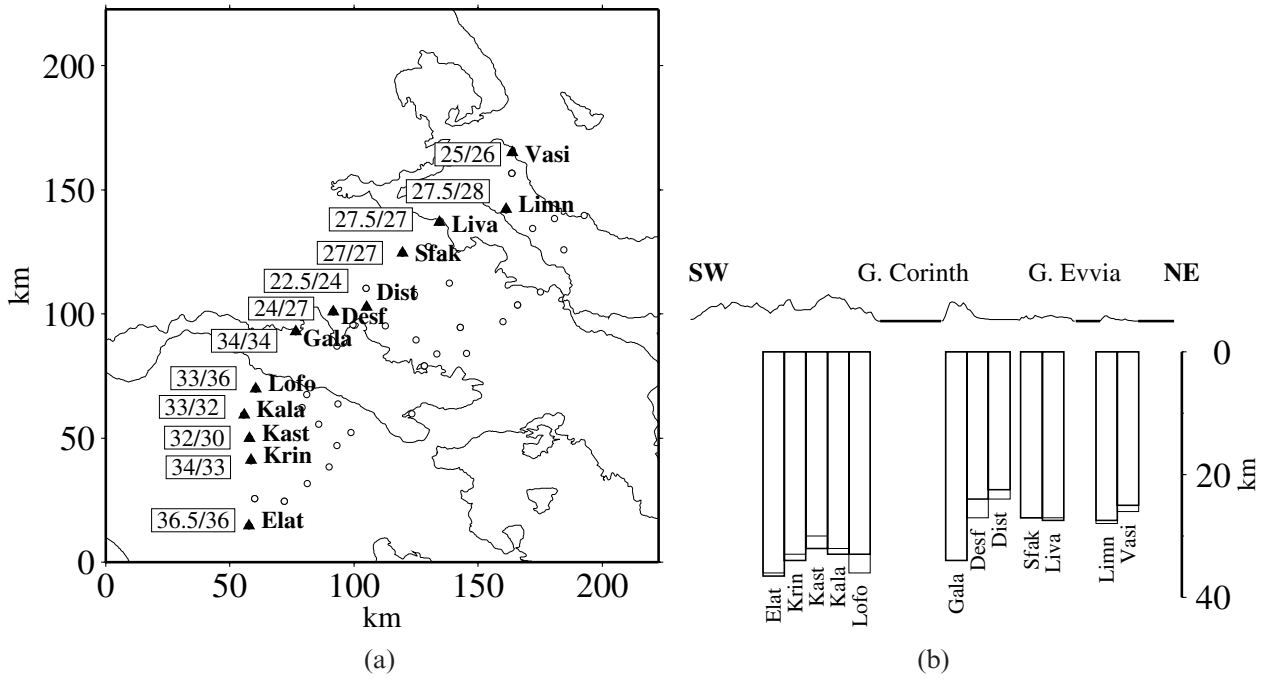

Figure 8. Comparison between the Moho depth variations from the receiver function analysis and gravity inversion. (a) First depth is from receiver function, second one is from gravity. (b) SW–NE cross-section through the seismological experiment showing Moho depth below each three-component seismological station. Thick line is Moho depth from receiver function, thin line is from gravity inversion.

from our gravity inversion). The minimum Moho depth (22.5 km from the receiver function analysis and about 25 km from gravity) is reached beneath the northern coast of Corinth (beneath station DIST). Towards Evvia, the receiver function analysis indicates a slightly deeper Moho at about 27 km depth, which is still consistent with the gravity inversion results (Fig. 8).

4 DISCUSSION

The aim of this study was to image the Moho topographic variations beneath the Corinth area. The results of gravity inversion, consistent with independent seismological observations, show two main features (Fig. 6): crustal thickening in the southwestern part of the region and several areas of smaller-scale crustal thinning. The question that arises now is how do these Moho variations relate to the structures seen at the surface and/or to the rifting process?

It is possible to associate the deep Moho in the western part of the region with the compensation of the Hellenides, which trend NNW–SSE. In an Airy model, the crustal thickening beneath elevations of 1.5–2 km would be similar to that obtained from inversion (about 10 km). The other striking feature we obtained is the zones of thinner crust. They are regularly spaced at about 60 km and trend in a NW–SE direction (Fig. 6). These features are located south and north of Corinth and near the Evvia Gulf (stations KAST and DIST, Fig. 8). They do not obviously correspond to structures at the surface (i.e. the Corinth or Evvia Rift). Resolving the location and amount of crustal thinning is difficult in the Gulf of Evvia because there are neither gravity measurement points nor seismological stations. The gravity inversion shows a zone of thin crust to the south of the Corinth Rift. The receiver function analysis is limited by the location of the profile and the tomographic results only show a small increase of the velocity. From both gravity and tomography results, this crustal thinning appears to be the western end of a NNW-striking structure that reaches the Gulf of Argos towards the southeast (Fig. 1). A wider network of seismological stations would increase our confidence in the interpretation here.

The crustal thinning beneath DIST (Fig. 8) that we observed lies to the north of the Gulf of Corinth (Fig. 6). All studies show a crustal thinning between 4 and 6 km over a width of about 20 km. The present Corinth Rift is thought to be the result of a reactivation that started only 1 Myr ago (Armijo *et al.* 1996). Although the extension rate is high (1–1.5 cm yr^{-1} after Briole *et al.* 2000), it is unlikely to have produced such crustal thinning in 1 Myr only by normal faulting across the upper crust. When compared to the whole Aegean extension, for instance, the crust there was thinned by about 10 km in 15–20 Myr (e.g. Makris 1978; Papazachos & Nolet 1997). One has thus to consider rheological properties in the lower crust such as ductile deformation and/or crustal faulting along a low-angle detachment plane. Moreover, the NW–SE-trending direction of this crustal thinning is slightly oblique to the trend of the Corinth Rift, but similar to Miocene extensional structures (e.g. Jolivet & Patriat 1999).

We thus propose that this crustal thinning began in the Miocene, 15–20 Myr ago, and that the present Corinth Rift became active more recently, as proposed by Armijo *et al.* (1996).

4.1 Aegean evolution and boudinage

In Miocene times, around 15–20 Myr ago, the SW–NE extension of the Aegean region started (Fig. 9a), probably by gravitational collapse (Le Pichon *et al.* 1995). This extension could have occurred by boudinage due to the large lateral

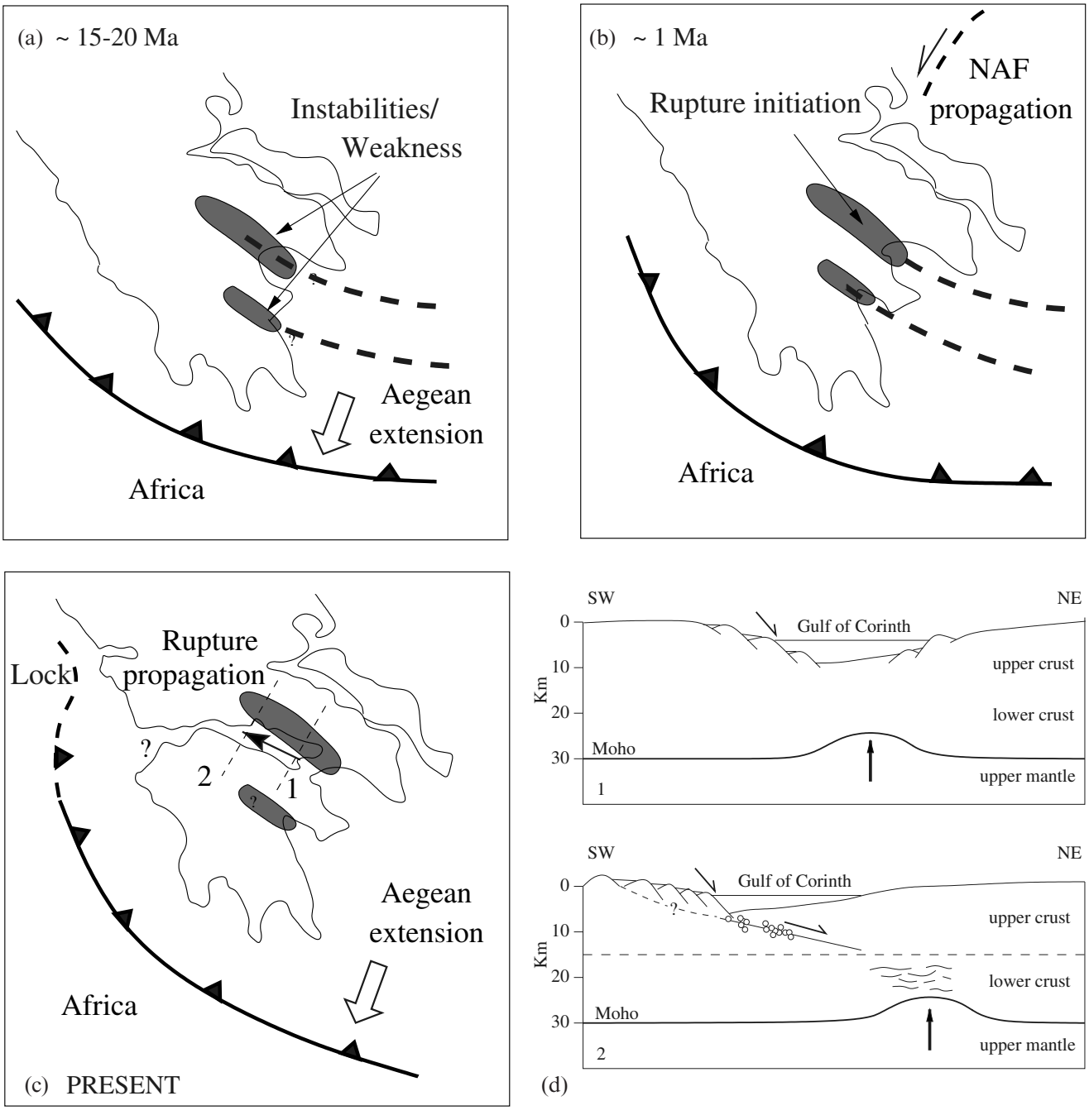

Figure 9. Proposed geodynamical evolution of the region from Miocene time to present. (a) Miocene time: the extension of Aegean lithosphere created regularly spaced instabilities (boudinage effect). The open arrow indicates the direction of Aegean extension. (b) Crustal rupture initiation was favoured in these weakened areas, which were reactivated 1 Myr ago. (c) At present, the observed offset between the maximum crustal thinning and the surface location of the Gulf of Corinth may be explained by changes in boundary conditions. The black arrow indicates the direction of rupture propagation. (d) This offset is also consistent with the idea of a crustal low-angle normal fault at about 12 km depth, accommodating the asymmetry of the rift in its western part. The deformation in the lower crust can be accounted for by ductile deformation (lines in the sketch). The circles represent the microseismicity from a 2 month experiment in this part of the rift (Rigo *et al.* 1996).

dimension of the thickened continental lithosphere (Martinod & Davy 1992; Armijo *et al.* 1996). We propose that the spatial periodicity of the three areas of crustal thinning detected by this study in the Corinth and Evvia areas may also indicate such lithospheric instabilities (Fig. 9a). Crustal ruptures could have thus been favoured in these specific necking zones, such as in the Corinth and Evvia areas (Fig. 9b).

In the boudinage process, the wavelength of the deformation is expected to be four–six times the thickness of the competent layers and is also controlled by the extent to which these layers are coupled (e.g. Ricard & Froidevaux 1986; Martinod & Davy 1992; Cloetingh & Burov 1996). Since the zones of crustal thinning are spaced at 60 km (Fig. 6), we expect the elastic layer to be about 10–15 km thick. This result is in good agreement

with the estimated effective elastic thickness (EET) in this region (King *et al.* 2000). We also note that it corresponds to the seismogenic layer deduced from previous seismological studies (Rietbrock *et al.* 1996; Rigo *et al.* 1996). Rietbrock *et al.* (1996) used microseismicity and focal mechanisms to show that a low-angle detachment surface is likely to exist at about 12 km depth, which may separate the elastic upper crust from the ductile lower crust. This is consistent with a very strong conductivity discontinuity evidenced beneath Corinth at about 10 km depth by magnetotelluric soundings (Pham *et al.* 1996). Thermomechanical modelling could be used at this point to express this in terms of the rheology of the crustal and mantle lithosphere in the Aegean region.

4.2 The Gulf of Corinth Rift

After this first stage of extension, which led to periodic crustal thinning, the Gulf of Corinth initiated around 1 Myr ago (Fig. 9b), possibly by the propagation of the North Anatolian fault (Armijo *et al.* 1996). The westward propagation of this fault is a potential cause for the present high extension rate. The Corinth Rift is likely to propagate westwards (Clarke *et al.* 1997), suggesting that the Gulf initiated in its eastern part (Fig. 9b).

As the rift probably initiated where the crust was thin, one might expect the Gulf of Corinth to strike in the same direction as the crustal thinning. However, this is not the case: the active Corinth Rift is clearly oblique to Miocene crustal thinning (Fig. 6). Several explanations may account for this offset. First, upper crustal discontinuities related to the Hellenic fabric may be reactivated. Unfortunately, the extension at depth of these structures is not well enough known to investigate this possibility. However, the surficial expressions of predominant structures do not trend in this direction. Second, a change in boundary conditions between Miocene and Quaternary times could have modified the rupture propagation. The continental collision that took place north of Kefalinia (Fig. 1) could have locked the rifting propagation northwestwards and forced extension to occur in a more N–S direction (Fig. 9c). This may also explain the difference in present-day seismic activity between Corinth and Evvia. Although the Evvia Rift is nearer to the North Anatolian Fault, it is less active than the Corinth Rift. The inherited fabric, as well as the NW continental collision, may play an important role, favouring strain accommodation across the Corinth area rather than in the Gulf of Evvia.

As far as the rifting process is concerned, we propose a combined mechanism (pure and simple shear) that can account for both the seismological observations and the offset observed between the crustal thinning and the rifting surface location. Unlike Wernicke (1985), who considered a lithospheric low-angle normal fault to accommodate the offset between crustal thinning and surface rifting, we propose a model with a low-angle normal fault in the upper crust and with ductile deformation in the lower crust (Lister & Davis 1989). The offset between shallow and deeper structures may be accommodated by the low-angle normal fault (Fig. 9d) at about 12 km depth (Rietbrock *et al.* 1996; Rigo *et al.* 1996). A more ductile crustal layer may partially contribute to the offset accommodation and rifting extension from about 10–15 km depth. This agrees with the rheological deductions made from the boudinage wavelength and the lack of seismicity below this limit. This asymmetry is also a tempting explanation for the different crustal deformation mechanisms in the eastern and western parts of the Gulf of Corinth. Shallow (about 30°) north-dipping fault planes have been detected at depth beneath the western part of the Corinth Rift (Rietbrock *et al.* 1996; Bernard *et al.* 1997) and may correspond to the low-angle normal fault at 12 km depth that we propose here for the combined rifting mode. The extensional faults that crop out south of the gulf are steeper (45–50°) and may connect with the low-angle plane at depth (Rigo *et al.* 1996; Sorel 2000). In the eastern part of the rift, 45–50° fault plane solutions are reported (Jackson *et al.* 1982; Taymaz *et al.* 1991). They may be related to normal faults exposed at the surface, and may correspond to another mode of deformation in the lower crust (Fig. 9d). The offset between surface rupture and deep extensional processes disappears as we go eastwards, and accommodation along a detachment surface is no longer necessary. Extension can then be accounted for by steeper normal faulting and/or ductile deformation in the lower crust.

However, the evolution of the westernmost part of the Corinth Rift remains undefined. The offset between deep and shallow structures becomes so large that a low-angle normal fault is unlikely to accommodate it.

5 CONCLUSIONS

The primary objective of this study was to provide new insight into the understanding of the continental rifting process in the Aegean region. Critical to this objective was the Moho topography imaged by gravity inversion beneath the Corinth Rift area. Complementary results come from tomographic and receiver function analyses presented elsewhere (Tiberi *et al.* 2000; Schubnel 1999). The outcomes of these three independent studies are consistent and increase the confidence in our results.

A thick crust of the order of 40 km in the western part of the Gulf of Corinth results from the isostatic compensation of the Hellenides mountains. As we go eastwards, the crust thins to about 25 km. Superimposed on this large-scale gradient, three zones of crustal thinning, each trending NW–SE and about 15–20 km wide, are spaced at about 60 km intervals across the study area. Boudinage processes during the Aegean Miocene extension (15–20 Ma) could have created the periodicity of these structures. Then, some of these areas such as the Gulf of Corinth were preferentially reactivated 1 Myr ago, possibly by the westward propagation of the North Anatolian Fault (Armijo *et al.* 1996). The maximum crustal thinning observed (about 4–6 km) is located beneath the northern edge of the Gulf of Corinth, and is displaced from the surface location of the rifting structures. Inherited fabric or changes in boundary conditions may explain this offset, which can be accommodated by a crustal subhorizontal normal fault at about 12 km depth. This idea agrees with results from previous seismological studies (Rietbrock *et al.* 1996; Rigo *et al.* 1996) and is consistent with the asymmetrical combined rifting mode proposed by Lister & Davis (1989).

As shown in this work, the combined use of gravity and seismological studies provides an efficient means to investigate lithospheric structures. In order to shed more light on the mechanisms of this continental extension, it will be of prime interest to carry out a gravity inversion on a larger scale to determine whether the crustal thinning periodicity we observe in the area of Corinth and Evvia continues across the Aegean area as suggested by Armijo *et al.* (1996).

ACKNOWLEDGMENTS

We are grateful to Hélène Hébert and Roger Hiking for helpful discussions on the Oldenburg algorithm. We benefited from discussion with Rolando Armijo, Genia Burov, Alfred Hirn and Laurent Jolivet. We thank Harmen Bijwaard and Wim Spakman for providing us with their tomographic model, and Alexandre Schubnel for the results of the receiver function analysis. This paper benefited from the comments of two anonymous reviewers. TK was supported by NERC grant GT4/93/179G and GEP loan 437/1094. This is IPGP contribution number 1737.

REFERENCES

Aki, K., Christoffersson, A. & Husebye, E.S., 1977. Determination of the three-dimensional seismic structure of the lithosphere, *J. geophys. Res.,* **82,** 277–296.

Allemand, P. & Brun, J.-P., 1991. Width of continental rifts and rheological layering of the lithosphere, *Tectonophysics,* **188,** 63–69.

Ambraseys, N. & Jackson, J., 1990. Seismicity and associated strain of central Greece between 1890 and 1988, *Geophys. J. Int.,* **101,** 663–708.

Armijo, R., Meyer, B., King, G., Rigo, A. & Papanastassiou, D., 1996. Quaternary evolution of the Corinth Rift and its applications for the late Cenozoic evolution of the Aegean, *Geophys. J. Int.,* **126,** 11–53.

Barka, A., 1996. Slip distribution along the North Anatolian fault associated with the large earthquakes of the period 1939 to 1967, *Bull. seism. Soc. Am.,* **86,** 1238–1254.

Bernard, P., *et al.*, 1997. The *Ms* = 6.2, June 15, 1995 Aigion earthquake (Greece): evidence for low normal faulting in the Corinth rift, *J. Seism.,* **1,** 131–150.

Bijwaard, H., Spakman, W. & Engdahl, E., 1998. Closing the gap between regional and global travel time tomography, *J. geophys. Res.,* **103,** 30 055–30 078.

Billiris, H., *et al.*, 1991. Geodetic determination of tectonic deformation in central Greece from 1900 to 1988, *Nature,* **350,** 124–129.

Birch, F., 1961. The velocity of compressional waves in rocks to 10 kilobars, part 2, *J. geophys. Res.,* **66,** 2199–2224.

Bonneau, M., 1982. Évolution géodynamique de l'arc égéen depuis le Jurassique supérieur jusqu'au Miocène, *Bull. Soc. Géol. Fr.,* **24,** 229–242.

Briole, P., *et al.*, 2000. Active deformation of the Corinth Rift, Greece: results from repeated GPS surveys between 1990 and 1995, *J. geophys. Res.,* **105,** 25 605–25 625.

Brun, J.-P. & Beslier, M., 1996. Mantle exhumation at passive margins, *Earth planet. Sci. Lett.,* **142,** 161–173.

Christensen, N. & Mooney, W., 1995. Seismic velocity structure and composition of the continental crust: a global view, *J. geophys. Res.,* **100,** 9761–9788.

Ciminale, M. & Loddo, M., 1989. A computer program to perform the upward continuation of potential field data between arbitrary surfaces, *Comput. Geosci.,* **15,** 889–903.

Clarke, P., *et al.*, 1997. Geodetic estimate of seismic hazard in the Gulf of Korinthos, *Geophys. Res. Lett.,* **24,** 1303–1306.

Clarke, P., *et al.*, 1998. Crustal strain in central Greece from repeated GPS measurements in the interval 1989–1997, *Geophys. J. Int.,* **135,** 195–214.

Cloetingh, S. & Burov, E., 1996. Thermomechanical structure of European continental lithosphere: constraints from rheological profiles and EET estimates, *Geophys. J. Int.,* **124,** 695–723.

Evans, J.R. & Achauer, U., 1993. Teleseismic velocity tomography using the ACH method: theory and application to continental-scale studies, in *Seismic Tomography: Theory and Practice,* pp. 319–360, eds Iyer, H. & Hirahara, K., Chapman & Hall, New York.

Gregersen, S. & Jæger, W., 1984. The gravity field of a dipping plate in Greece, *Geophys. J. R. astr. Soc.,* **76,** 439–443.

Hébert, H., Deplus, C., Huchon, P., Khanbari, K. & Audin, L., 2000. Lithospheric structure of the nascent spreading ridge inferred from gravity data: the western Gulf of Aden, *J. geophys. Res.,* in press.

Henkel, H., Lee, M. & Lund, C., 1990. An integrated geophysical interpretation of the 200 km FENNOLORA section of the Baltic Shield, in *The European Geotraverse: Integrative Studies,* pp. 1–47 eds Freeman, R., Giese, P. & Mueller, S., European Science Foundation, Strasbourg, France.

Hubert, A., King, G., Armijo, R., Meyer, B. & Papanastasiou, D., 1996. Fault reactivation, stress interaction and rupture propagation of the 1981 Corinth earthquake sequence, *Earth planet. Sci. Lett.,* **142,** 573–585.

Jackson, J., Gagnepain, J., Houseman, G., King, G., Papadimitriou, P., Soufleris, C. & Virieux, J., 1982. Seismicity, normal faulting, and the geomorphological development of the Gulf of Corinth (Greece): the Corinth earthquakes of February and March 1981, *Earth planet. Sci. Lett.,* **57,** 377–397.

Jolivet, L. & Patriat, M., 1999. Ductile extension and the formation of the Aegean Sea, in *The Mediterranean Basins: Tertiary Extensions Within the Alpine Orogen,* eds Durand, B., Jolivet, L., Horvath, F. & Séranne, M., *Geol. Soc. Spec. Publ.*, **156,** 427–456.

King, T., 1998. Mechanisms of isostatic compensation in areas of lithospheric extension: examples from the Aegean, *PhD thesis,* University of Leeds, Leeds.

King, T., Ebinger, C., Stark, C. & Collier, R., 2000. Effective elastic thickness across the Aegean, *J. geophys. Res.,* submitted.

Le Pichon, X. & Angelier, J., 1979. The Hellenic arc and trench system: a key to the neotectonic evolution of the eastern Mediterranean area, *Tectonophysics,* **60,** 1–42.

Le Pichon, X., Chamot-Rooke, N. & Lallemant, S., 1995. Geodetic determination of the kinematics of central Greece with respect to Europe: implication for eastern Mediterranean tectonics, *J. geophys. Res.,* **100,** 12 675–12 690.

Lister, G. & Davis, G., 1989. The origin of metamorphic core complexes and detachment faults formed during Tertiary continental extension in the northern Colorado River region, U.S.A., *J. struct. Geol.,* **11,** 65–94.

Lundgren, P., Giardini, D. & Russo, R.M., 1998. A geodynamic framework for eastern Mediterranean kinematics, *Geophys. Res. Lett.,* **25,** 4007–4010.

Mahatsente, R., Jentzsch, G. & Jahr, T., 1999. Crustal structure of the Main Ethopian Rift from gravity data: 3-dimensional modeling, *Tectonophysics,* **313,** 363–382.

Makris, J., 1978. The crust and upper mantle of the Aegean region from deep seismic soundings, *Tectonophysics,* **46,** 269–284.

Martinod, J. & Davy, P., 1992. Periodic instabilities during compression or extension of the lithosphere, 1, Deformation modes from an analytical perturbation method, *J. geophys. Res.,* **97,** 1999–2014.

McClusky, S., *et al.*, 2000. Global Positioning System constraints on plate kinematics and dynamics in the eastern Mediterranean and Caucasus, *J. geophys. Res.,* **105,** 5695–5719.

McKenzie, D., 1978a. Active tectonics of the Alpine-Himalayan belt: the Aegean Sea and surroundings regions, *Geophys. J. R. astr. Soc.,* **55,** 217–254.

McKenzie, D., 1978b. Some remarks on the development of sedimentary basins, *Earth planet. Sci. Lett.,* **40,** 25–32.

Mercier, J., 1981. Extensional-compressional tectonics associated with the Aegean Arc: comparison with the Andean Cordillera of south Peru-north Bolivia, *Phil. Trans. R. Soc. Lond.,* A**300,** 337–355.

Oldenburg, D., 1974. The inversion and interpretation of gravity anomalies, *Geophysics,* **39,** 526–536.

Ori, G.G., 1989. Geologic history of the extensional basin of the Gulf of Corinth (? Miocene-Pleistocene), Greece, *Geology,* **17,** 918–921.

Papazachos, C. & Kiratzi, A., 1996. A detailed study of the active crustal deformation in the Aegean and surrounding area, *Tectonophysics,* **253,** 129–153.

Papazachos, C. & Nolet, G., 1997. *P* and *S* deep velocity structure of the Hellenic area obtained by robust nonlinear inversion of travel times, *J. geophys. Res.,* **102,** 8349–8367.
Parker, R., 1972. The rapid calculation of potential anomalies, *Geophys. J. R. astr. Soc.,* **31,** 447–455.
Petit, C., Burov, E. & Déverchère, J., 1997. On the structure and mechanical behaviour of the extending lithosphere in the Baikal Rift from gravity modelling, *Earth planet. Sci. Lett.,* **149,** 29–42.
Pham, V.N., Boyer, D., Chouliaras, G. & Bernard, P., 1996. Conductivité électrique et structure de la croûte dans la région du Golfe de Corinthe (Grèce) d'après les résultats de sondage Magnéto-Tellurique (SMT), *C. R. Acad. Sci. Paris,* **323,** 651–656.
Ricard, Y. & Froidevaux, C., 1986. Stretching instabilities and lithospheric boudinage, *J. geophys. Res.,* **91,** 8314–8324.
Rietbrock, A., Tiberi, C., Scherbaum, F. & Lyon-Caen, H., 1996. Seismic slip on a low angle normal fault in the Gulf of Corinth: evidence from high-resolution cluster analysis of microearthquakes, *Geophys. Res. Lett.,* **23,** 1817–1820.
Rigo, A., Lyon-Caen, H., Armijo, R., Deschamps, A., Hatzfeld, D., Makropoulos, K., Papadimitriou, P. & Kassaras, I., 1996. A microseismic study in the western part of the Gulf of Corinth (Greece): implications for large-scale normal faulting mechanisms, *Geophys. J. Int.,* **126,** 663–688.
Roberts, S. & Jackson, J., 1991. Active normal faulting in central Greece: an overview, in *The Geometry of Normal Faults,* eds Roberts, A.M., Yielding, G. & Freeman, B., *Geol. Soc. Spec. Publ.,* **56,** 125–142.
Ruppel, C., 1995. Extensional processes in continental lithosphere, *J. geophys. Res.,* **100,** 24 187–24 215.
Schubnel, A., 1999. Étude de la transmission des ondes Ps dans le Golfe de Corinthe, variations latérales et structures de la croûte, *DEA,* Université Paris 7.
Sorel, D., 2000. A Pleistocene and still-active detachment fault and the origin of the Corinth-Patras rift (Greece), *Geology,* **28,** 83–86.
Taymaz, T., Jackson, J. & McKenzie, D., 1991. Active tectonics of the north and central Aegean Sea, *Geophys. J. Int.,* **106,** 433–490.
Tiberi, C., 1999. Rifts de Corinthe et d'Evvia (Grèce): structure lithosphérique par tomographie télésismique et gravimétrie, *PhD thesis,* Université Paris 7, Paris.
Tiberi, C., *et al.*, 2000. Crustal and upper mantle structure beneath the Corinth rift (Greece) from a teleseismic tomography study, *J. geophys. Res.,* **105,** 28 159–28 172.
Truffert, C., Chamot-Rooke, N., Lallemant, S., De Voogd, B., Huchon, P. & Le Pichon, X., 1993. the crust of the Western Mediterranean Ridge from deep seismic data and gravity modelling, *Geophys. J. Int.,* **114,** 360–372.
Tsokas, G. & Hansen, R., 1997. Study of the crustal thickness and subducting lithosphere in Greece from gravity data, *J. geophys. Res.,* **102,** 20 585–20 597.
Wernicke, B., 1985. Uniform-sense normal simple shear of continental lithosphere, *Can. J. Earth Sci.,* **22,** 108–125.

APPENDIX A: SYNTHETIC TESTS

We present here one of several synthetic tests we carried out to investigate possible artefacts coming from the gravity inversion method of Oldenburg (1974). We first generate a gravity anomaly from a 3-D synthetic model corresponding to a defined Moho

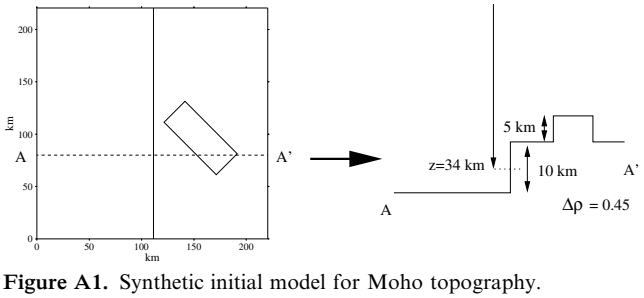

Figure A1. Synthetic initial model for Moho topography.

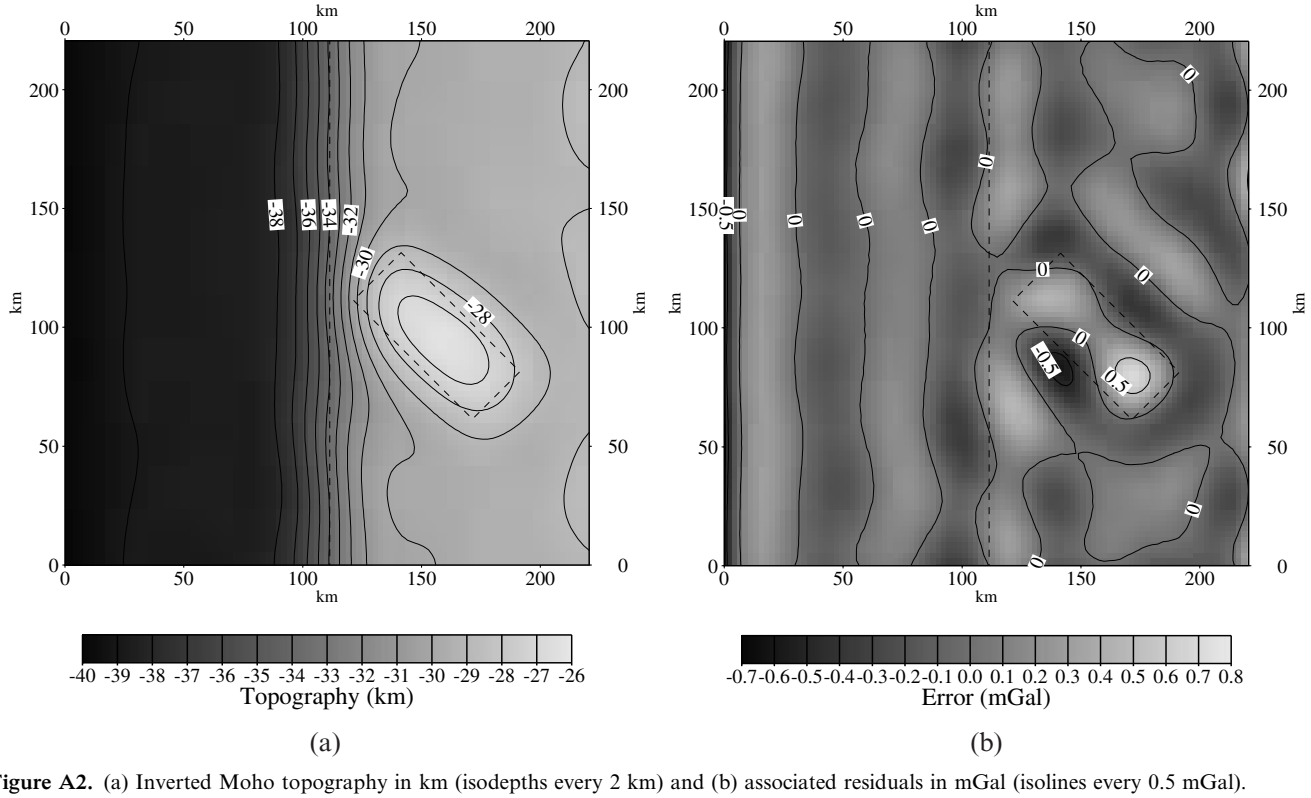

Figure A2. (a) Inverted Moho topography in km (isodepths every 2 km) and (b) associated residuals in mGal (isolines every 0.5 mGal).

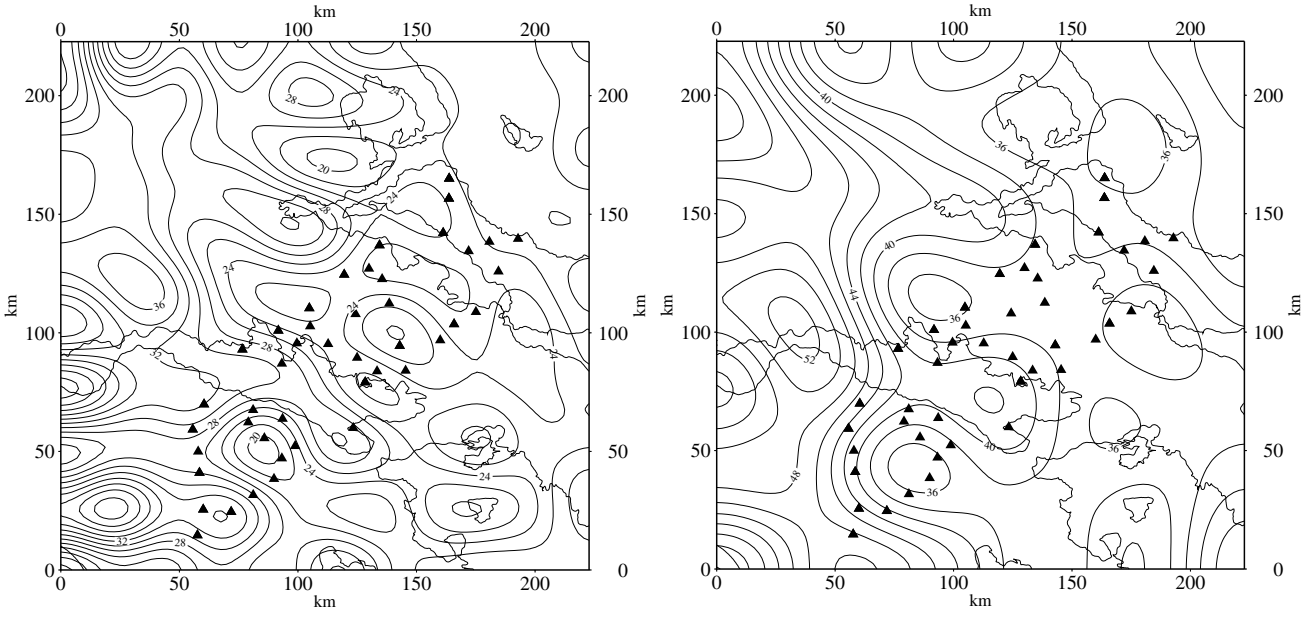

Figure B1. Moho topography in km for (a) $z_0 = 26$ km, cosine taper between 55 and 65 km and (b) $z_0 = 40$ km, cosine taper between 85 and 105 km. Isodepth every 2 km, map in UTM coordinates (km).

topography (Fig. A1). A rectangular structure superimposed on an abrupt step-like structure is used. Gravity anomalies are calculated using a 450 kg m^{-3} density contrast. Wavelengths shorter than 65 km are filtered out. The inverted Moho topography is shown in Fig. A2 with the associated residuals. The inversion converges after seven iterations and the final rms is 0.18 mGal.

It is clear that the general features and topographic variations are well reproduced in both position and amplitude. Both structures (step-like and rectangular) are well separated from each other. The amplitude of the top of the topography (initially at 24 km depth) is slightly underestimated (26 km for the resulting topography), consistent with positive residuals (Fig. A2).

A short-wavelength signal is present and contaminates the result. This signal is also present in the residuals, and does not correspond to real structures. Even though we mirror the data prior to Fourier transforming it, it probably comes from the use of the Fourier transform on a step-like structure. Thus, one has to be careful when interpreting short wavelengths in the inverted Moho topography. However, the amplitude of this short-wavelength signal is quite small, much smaller than that obtained from our data.

APPENDIX B: TESTS FOR INVERSION STABILITY

Different values of z_0 were tested for the inversion scheme, and we present in this section the results obtained for two values, $z_0 = 26$ km and $z_0 = 40$ km. We adjust the filter to the values of z_0 and we obtain the Moho variations shown in Fig. B1. The cosine taper was applied between 55 and 65 km for $z_0 = 26$ km, and between 85 and 105 km for $z_0 = 40$ km. The crust–mantle density contrast used for both cases was 450 kg m^{-3}. One can see that the main features remain stable: a crustal thickening in the western part of the region and NW–SE-trending areas of crustal thinning about 15 km wide in the eastern part. Only the wavelengths are different, due to the shallower or deeper Moho reference depth z_0. The magnitude of the crustal thinning and thickening is about the same. For a fixed z_0 and a $\Delta\rho$ of 350 kg m^{-3}, the wavelengths remain the same, but the magnitude of Moho variations is enhanced by about 2 km.